

Spectral Signature of Landscape Channelization

Milad Hooshyar^{1,2,3}, Gabriel Katul⁴ and Amilcare Porporato^{1,2}

¹Princeton Environmental Institute, Princeton University

²Department of Civil and Environmental Engineering, Princeton University

³Princeton Institute for International and Regional Studies, Princeton University

⁴Nicholas School of the Environment and the Department of Civil and Environmental Engineering, Duke University

Key Points:

- The elevation spectrum contains a power-scaling in a wide range of scales.
- Dimensional and self-similarity arguments connect the power-scaling of the spectrum to the nonlinearity of erosion term.
- Numerical simulation and data from a physical experiment are used to validate our results.

Corresponding author: Milad Hooshyar, hooshyar@princeton.edu

Abstract

Channel networks increase in complexity as the importance of erosion grows compared to diffusion by soil creep, giving rise to a channelization cascade. In this cascade, smaller channels join to form progressively larger ones with an alternation of ridges and valleys involving a multitude of wavelengths. Simulations of landscape evolution models and laboratory experiments are used to uncover the signature of such a cascade in the wavenumber spectrum of elevation fluctuations. Power spectra at intermediate distances from the boundaries are characterized by a peak wavenumber (i.e., the most energetic mode) that is related to the quasi-cyclic valleys superimposed on power-law scaling with exponent (α) across a wide range of smaller scales. Dimensional analysis and self-similarity arguments are used to reveal the controlling factors on α , showing that α is uniquely linked to the power-law relation (with exponent m) between erosion potential and the specific drainage area via $\alpha = 2m - 3$.

Plain Language Summary

Landscapes exhibit a periodic valley spacing at the interface of the channelization phase transition. As the importance of erosion grows, quasi-cyclic valleys emerge with a characteristic power-law scaling in the elevation spectrum across a wide range of scales. We use dimensional analysis and self-similarity arguments to show that the exponent of this power-scaling α is uniquely linked to the power-law relation (with exponent m) between erosion potential and the specific drainage area. This result is validated in numerical simulation and using data from a physical experiment.

1 Introduction

Landscape channelization starts at the critical point where erosion overcomes the smoothing effects of the diffusive soil creep (Sweeney et al., 2015; Perron, Dietrich, & Kirchner, 2008; Bonetti et al., 2020). Below this critical point, the landscape is without channels, while just above it, regularly spaced channels form (Perron, Dietrich, & Kirchner, 2008; Perron et al., 2009), defining an emergent length scale of erosional landscapes (Perron et al., 2009). As the importance of erosion further increases, the surface becomes progressively complex forming a hierarchy of interconnected valley and ridge networks (Bonetti et al., 2020). In the highly channelized regime, the topographic surface exhibits several scaling laws (Rodríguez-Iturbe & Rinaldo, 2001; Horton, 1945; Strahler, 1952) and self-similar statistical properties typical of branch-forming and out-of-equilibrium systems in statistical physics (Sinclair & Ball, 1996; Rinaldo et al., 1996; Banavar et al., 1997, 2001; Witten & Sander, 1983; Goldenfeld & Shih, 2017; Kramer & Marder, 1992; Arneodo et al., 1992). Moreover, the valley spacing is no longer regular and acquires a statistical connotation, resulting from a superposition of modes of landscape fluctuations linked to both geomorphological characteristics and external geometrical constraints (i.e., boundary conditions in numerical simulations or large scale geology in natural topography).

Understanding the interplay of the factors determining the properties of this progression from deterministic to statistical regularity of the valley-ridge topography appears as a fundamental problem having both theoretical and practical implications. Besides the already mentioned work on regular valley spacing (Perron, Dietrich, & Kirchner, 2008; Perron et al., 2009), previous literature also analyzed specific aspects of the spectral signature of channelization in relation to the characteristic length scale (Perron, Kirchner, & Dietrich, 2008), the self-similarity across scales (Passalacqua et al., 2006), and the related fractal dimensions (Newman & Turcotte, 1990; Huang & Turcotte, 1989). To bridge the previous work on valley spacing and self-similar landscape variability, in this paper, we consider the linkages among the spectral properties of landscape transects, their scaling laws, and the dominant ridge-valley mode. To this purpose, a landscape power spectrum can be defined considering elevation variations along one-dimensional (longi-

tudinal) transects in which the total 'energy' content is the variance associated with these variations (Perron, Kirchner, & Dietrich, 2008; Passalacqua et al., 2006). At the critical point of channel formation, the surface contains periodic channels (see the comprehensive analysis in (Perron, Dietrich, & Kirchner, 2008; Perron et al., 2009)) and the elevation variance becomes concentrated around the wavenumber of the regular channel spacing (Bonetti et al., 2020). Beyond the critical point, landscape channelization enables the transfer of sediment or water flux to form a channel hierarchy, which presumably corresponds to an 'energy' cascade in the landscape spectrum due to the nonlinear coupling across different modes of variability of the landscape evolution equations.

Regarding the role of these aforementioned nonlinearities, several studies on elevation spectra of 1-dimensional transects report power-law decay of energy across scales with an exponent close to -2 (Newman & Turcotte, 1990; Huang & Turcotte, 1989). This is a rather intriguing result since such scaling is characteristic of classical Brownian noise (Turcotte, 1987; Bell Jr, 1975) and corresponds to a Lorentzian spectrum (Berg-Sørensen & Flyvbjerg, 2004), implying an exponential decay of the elevation autocorrelation with increasing spatial lag. Taken at face value, these clues would suggest an underlying linear stochastic dynamics, at odds with the presence of nonlinear terms responsible for the very formation of the channel network. A plausibility argument to explain this oddity is that increases in landscape complexity are accompanied by a reduction of the effect of nonlinearity. This conjecture is thus related to whether the activation of many degrees of freedom at high channelization regimes may elicit some form of statistical regularity capable of obfuscating the role of nonlinearities acting at small scales within each valley-ridge pair.

To address at least in part this conjecture, a link between the spectral signature of surface channelization and the basic parameters describing a landscape evolution model is needed. In simulated surfaces within a long rectangular domain, the spectrum contains a well-defined peak that hints at a dominant channelization mode with a characteristic spacing. The wavenumber at the peak of this most energetic mode depends on the relative magnitude of erosion in relation to the exponent of the drainage area in the erosion law (denoted by m). At scales smaller than the spectral peak (higher wavenumbers), the energy content drops with a power-law scaling on a wide range of scales, highlighting the self-similarity and fractal behavior of elevation fluctuation. Starting from the spectrum of the regular valley regime, the power decay becomes flatter (spectrum widens) with increasing relative contribution of erosion. Especially interesting in this regard is the question of the possible existence of asymptotic behavior in the limit of high erosion rates and the appearance of a local, small scale regime of quasi-isotropy. In addition, the connection between spectral behavior of landscapes and basic geomorphologic parameters can connect the nonlinearity of erosion law to the power-law decay of spectrum and, in turn, to the fractal dimension of longitudinal elevation data (Huang & Turcotte, 1989; Voss, 1985).

2 Mathematical model and Simulations

The focus here is on a minimalist landscape evolution model (LEM) in the detachment-limited conditions (Izumi & Parker, 1995; Howard, 1994; Bonetti et al., 2020), where sediment redeposition is negligible. In this model, the change in surface elevation occurs due to diffusive soil creep, fluvial erosion, and tectonic uplift, according to

$$\frac{\partial z}{\partial t} = U + D\Delta z - Ka^m|\nabla z|, \quad (1)$$

where z is the elevation fields, U is the uplift rate and a is the specific drainage area (or drainage area per unit contour length). The diffusive soil creep is $D\Delta z$ and D is the soil diffusivity. The term $Ka^m|\nabla z|$ quantifies the fluvial erosion (sediment movement due to water flow) in which the constants m and K must be externally supplied. Eq. (1) is

coupled to the governing equation of the specific drainage area

$$\nabla \cdot \left(a \frac{\nabla z}{|\nabla z|} \right) = -1, \quad (2)$$

representing the steady-state continuity equation of water flow over a surface generated by a unitary rainfall with the assumption that water moves in the direction of the local slope with a constant velocity (Bonetti et al., 2018, 2020). Such assumptions are common to locally uniform free-surface open channel flow as expected from the Chezy or Manning type equations (Bonetti et al., 2017). The assumption of negligible sediment deposition in Eq. (1) is common in landscape evolution modeling; however, other formulations accounting for sediment redeposition have also been proposed (Smith & Bretherton, 1972; Willgoose et al., 1991; Davy & Lague, 2009). While the analysis here is restricted to detachment-limited conditions, the methodology based on dimensional and self-similarity arguments can be extended to models with different sediment transport formulations.

For a problem characterized by a single typical dimension l , the behavior of the system of Eqs. (1) and (2) is captured by a dimensionless number referred to as 'channelization index' and denoted by $\mathcal{C}_I = (Kl^{m+1}/D)$ where l is a typical length scale of the domain (Bonetti et al., 2020).

The coupled system formed by Eqs.(1) and (2) are solved numerically in a $l_x = 1500$ m by $l_y = 150$ m rectangular domain with zero-elevation at the boundaries ($z_\omega = 0$ m) as shown in Fig. 1a. The choice of a long domain (i.e., $l_x \gg l_y$) ensures that l_y is the dominant (or restrictive) length scale. Hence, the channelization index can be defined as $\mathcal{C}_I = Kl_y^{m+1}/D$. The numerical scheme uses an implicit approach to integrate the erosion term in Eq. (1). Details about the accuracy and efficiency of the numerical algorithm are featured elsewhere (Anand et al., 2019).

Fig. 1a and b compares the steady-state surfaces from numerical simulation for $\mathcal{C}_I = 10^3$ and 10^4 and $m = 0.5$. The formation and progression of channels have their imprint in the elevation field. As previously reported (Bonetti et al., 2020), with increasing \mathcal{C}_I the surface becomes progressively more dissected with a branched network of channels. Channels disappear in regions where the diffusive transport dominates over fluvial erosion mainly because of a small value of the specific drainage area.

Fig. 1c and d show the elevation along transects A-A and B-B, which are marked in Fig. 1a and b. The local minima in the elevation series correspond to channels, whereas the local maxima are ridges. The elevation series exhibits a quasi-cyclic behavior in which the dominant cycles correspond to the spacing of the main channels. With higher \mathcal{C}_I and as the surface becomes more channelized, the elevation fluctuations at smaller scales (higher wavenumbers) appear (see Fig. 1d). This finding is analogous to increasing the bulk Reynolds number (here \mathcal{C}_I) and the generation of finer Kolmogorov sized eddies in jets where the integral scale remains fixed (Tennekes et al., 1972).

3 Power Spectra

To address the study objective, connections between m , \mathcal{C}_I , and the spectral exponent of the longitudinal elevation series at preset y is sought. For this purpose, elevation fluctuations in wave-space are analyzed using the power-spectral density (PSD) of the longitudinal elevation series (along the x -axis) at a given y (denoted by $z_y(x)$) as

$$E(\omega) = |\hat{z}_y(\omega)|^2, \quad (3)$$

where

$$\hat{z}_y(\omega) = \int_x z(x) e^{-2\pi i \omega x} dx, \quad (4)$$

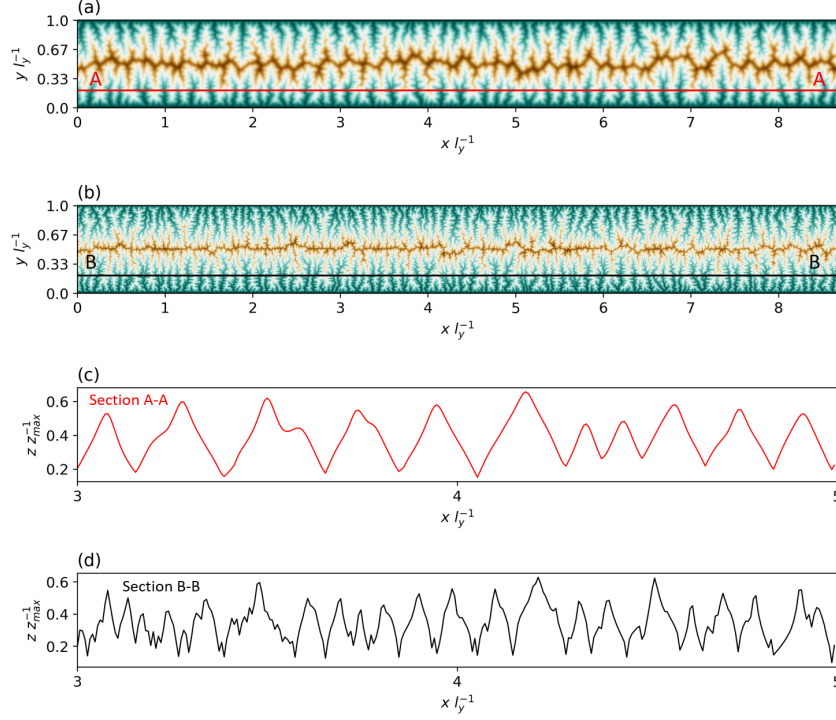


Figure 1. The steady-state numerical solution of Eqs.(1) and (2) for $m = 0.5$ and $C_I = 10^3$ in (a) and $C_I = 10^4$ in (b). The elevation along A-A and B-B transects are shown in (c) and (d). A rectangular domain ($l_x = 1500$ m by $l_y = 150$ m) with zero elevation at the boundaries ($z_\omega = 0$ m) is used. The first and last 100 m along the x -axis were removed for further analysis to approximate a semi-infinite domain.

is the Fourier transform of $z_y(x)$. Examples of z_y are shown in Fig. 1c and d for $y = 30$ m. Fig. 2a shows the stationary PSDs for the elevation series for different values of y covering the distance from the boundary and the domain's center in 5 m intervals. The PSDs exhibit approximate power-law scaling for almost a decade in the high wavenumber (small scale) ranges. The range of power-law scaling expands as y is moved away from the boundary. The corresponding wavenumber at which the PSDs' peak (i.e., energetic modes), denoted by ω_{max} , decrease (see the inset of Fig. 2a). For intermediate values of y , the PSDs appear independent of y , which allows isolating the effects of y by only devoting analysis to such an intermediate range of y .

Fig. 2b shows the PSD of elevation series at the intermediate distance from the boundary and domain center for a wide range of C_I and $m = 0.5$. Each line is the average of the PSDs for $0.07 \leq y l_y^{-1} \leq 0.27$ from the steady-state solutions. Two examples of such surfaces for $C_I = 10^3$ and 10^4 are shown in Fig. 1a and b. The change of C_I , which has previously been shown to modulate the channelization and mean-elevation profile (Bonetti et al., 2020; Hooshyar, Bonetti, et al., 2019), also impacts the distribution of energy of elevation fluctuations across scales. The PSDs also exhibit asymptotic behavior and collapse to a single curve at high C_I . It can be surmised that the PSDs become independent of C_I at high values analogous of C_I analogous to turbulent flow statistics becoming independent of Reynolds number at very high Reynolds numbers. The PSDs contain a visually evident power-law scaling at a wide range of scales, although their slopes vary with C_I . For each PSD, the exponent of the power-law scaling α is computed by fitting a piece-wise function to cover the rising limb at large frequencies, the intermit-

tent range with the power-law scaling, and the deviation at the fine scales. The inset of Fig. 2b shows the computed exponent for a range of \mathcal{C}_I . As \mathcal{C}_I increases, the power-law fits result in flatter exponents and saturate to a constant value for sufficiently large \mathcal{C}_I . The steepest PSD in the simulations correspond to $\mathcal{C}_I = 10^3$ with the exponent $\alpha \approx -4.2$ shown in Fig. 1b. The corresponding elevation series is shown in Fig. 1c and follows an almost triangular-shaped wave. It worth noting that for a perfectly triangular periodic wave function, the PSD decays following a power-law with exponent $= -4$.

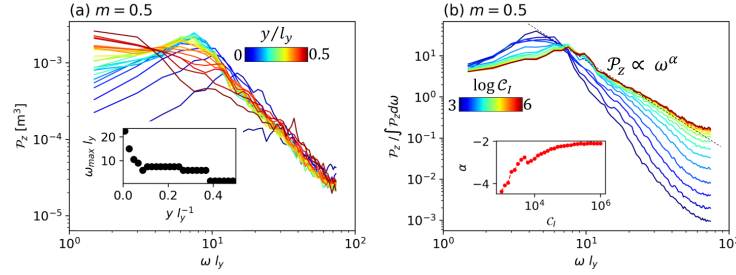


Figure 2. The PSD of elevation longitudinal series for steady-state surface variations. (a) shows PSDs for $\mathcal{C}_I = 10^5$ and $m = 0.5$ at different distance from the boundary, denoted by y covering the distance from the boundary to the domain's center in 3 m intervals. Each line corresponds to the average of the PSDs for all elevation signals within that interval. This inset shows the frequency at peak ω_{max} for different values of y . Quantities y and ω are normalized by l_y . (b) shows the PSDs for different values of \mathcal{C}_I for $m = 0.5$ at intermediate values of y (i.e., $0.07 \leq y l_y^{-1} \leq 0.27$). Each line corresponds to the average of the PSDs of all y within this range. The PSDs are normalized by the area under the spectrum for better visualisation. The inset shows the exponent α of power-law scaling fitted to the intermediate wavenumber for a range of \mathcal{C}_I .

The change of peak ω_{max} for $0.1 \leq m \leq 1$ and different values of \mathcal{C}_I is shown in Fig. 3. In general, ω_{max} exhibits a non-monotonic response to change in \mathcal{C}_I (Fig. 3) and m (Fig. 3b). The response of ω_{max} to change in \mathcal{C}_I depends on the value of m , whereby ω_{max} increases with \mathcal{C}_I for large m . For small values m , an increase in ω_{max} with \mathcal{C}_I is observed followed by a declining trend at high \mathcal{C}_I . The non-monotonic response to change in m is also highlighted in Fig. 3b in which an intermediate value of m maintains the smallest or biggest ω_{max} . Examples of numerically-simulated surfaces at selected values of m and \mathcal{C}_I are also shown in Fig. 3.

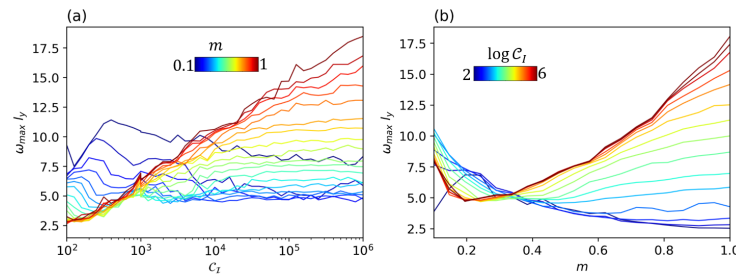


Figure 3. The response of ω_{max} to change in \mathcal{C}_I (a) and m (b). The peaks are calculated from PSDs at intermediate values of y (i.e., $0.07 \leq y l_y^{-1} \leq 0.27$).

4 Self-Similarity and Scaling

The dependence of the spectral scaling properties on the governing parameters can be analyzed with the aid of dimensional analysis (G. I. Barenblatt, 1996). For a longitudinal elevation series at a given y (see Figs. 1c and d), the amount of energy at a wavenumber ω at steady-state must vary with ω and variables described by Eq. 1. That is,

$$E(\omega) = g_1(\omega, y, l_y, D, K, U, m), \quad (5)$$

where g_1 is an unknown function. The energy $E(\omega)$ is defined over the fluctuations along the x -axis (see Eq. (3)); therefore, it has the dimension $[L_z^2 L_x]$ where L_z and L_x are lengths along z and x -axis. The ω represents a wavenumber along the x direction and has the dimension $[L_x^{-1}]$. The D , K , and U have the dimensions $[L_y^2 T^{-1}]$, $[L_y^{1-m} T^{-1}]$, and $[L_z T^{-1}]$ where T and L_y are dimensions of time and length along the y -axis. The y and l_y have a dimension $[L_y]$. At a sufficient distance from the boundary, it may be assumed that the information regarding the domain geometry and direction is lost; thus, length scales may become statistically isotropic, i.e., $L_x \equiv L_y$ (refer to Appendix I for details). This assumption is similar to local isotropy at small scales (or eddies detached from the boundary) of fully developed turbulent flow (Tennekes et al., 1972) and is further discussed in the following section.

Given three dimensions L_z , L_y , T and 7 dimensional governing variables, and choosing K , U , and ω as fundamental dimensionally independent variables guided by Eq. 1, the Buckingham II-theorem results in five Π groups. Stated differently, one of the Π groups (i.e. the one that contains $E(\omega)$ here) must then vary with the remaining three dimensionless groups. That is,

$$\frac{E(\omega) K^2 \omega^{3-2m}}{U^2} = g_2 \left(\frac{K \omega^{-(m+1)}}{D}, \omega l_y, \omega y, m \right). \quad (6)$$

A manipulation of Eq. (6) leads to

$$\frac{E(\omega) K^2 \omega^{3-2m}}{U^2} = g_3(\mathcal{C}_{\mathcal{I}}, \eta, \eta_\omega, m), \quad (7)$$

where $\mathcal{C}_{\mathcal{I}} = K l_y^{m+1}/D$ is the channelization index (Bonetti et al., 2020) defined earlier using the domain length scale l_y and quantifies the relative magnitude of erosion to diffusion, the quantity $\eta = K y^{m+1}/D$ has same form as that of $\mathcal{C}_{\mathcal{I}}$ but defined locally at y distance from the boundary, and $\eta_\omega = K \omega^{-(m+1)}/D$ is equivalent to η but defined in the frequency domain. In the asymptotic limit of relatively high $\mathcal{C}_{\mathcal{I}}$, η and η_ω must attain a near-constant limit away from the boundary. For this asymptotic limit, a hypothesis of complete self-similarity can be invoked in which g_3 is only a function of m ,

$$E(\omega) \propto \omega^{2m-3}, \quad (8)$$

where the proportionality coefficient is $(\frac{U}{K})^2 g_3(m)$. Eq. (8) predicts the exponent of the power spectral density that is independent of D and has a power-law decay. The condition of high $\mathcal{C}_{\mathcal{I}}$, η and η_ω is expected in systems that are dominated by erosion (high $\mathcal{C}_{\mathcal{I}}$), far enough from the boundary (high η), and within small enough scales (high η_ω). The assumption of complete self-similarity with respect to η and $\mathcal{C}_{\mathcal{I}}$ can be verified numerically. As shown in Fig. 2a at a distance far enough from the boundary (high η) the power-law scaling of PSD is robust. The collapse of PSDs at high $\mathcal{C}_{\mathcal{I}}$ in Fig. 2b also validates the self-similarity with respect to $\mathcal{C}_{\mathcal{I}}$.

Fig. 4a shows the PSDs of longitudinal elevation series in the intermediate range ($0.07 \leq y l_y^{-1} \leq 0.27$) from numerical simulation with $\mathcal{C}_{\mathcal{I}} = 10^5$ and $0.1 \leq m \leq 1$. Fig. 4b shows the exponent of the power fits to PSDs for simulations with $\mathcal{C}_{\mathcal{I}} \geq 10^5$, denoted by α , for different m values. This finding is, once again, in agreement with the relation $\alpha = 2m - 3$ in the intermediate range of m . This finding further corroborates

the validity of the assumption of complete self-similarity with respect to η_ω . Although an incomplete self-similarity or self-similarity of type two (G. Barenblatt & Goldenfeld, 1995) ($g_3 \propto \eta_\omega^\beta$) is also plausible, it does lead to a deviation from $\alpha = 2m - 3$.

It is to be noted that the deviation of numerical results from $\alpha = 2m - 3$ in Fig. 4 may be the result of channel-branching anisotropy that violates the assumption $L_x \equiv L_y$. For instance, if an anisotropy in length scales exists in the form of $L_x \equiv L_y^{1+\gamma}$, the assumption of complete self-similarity predicates $\alpha = 2m - 3 - \gamma$.

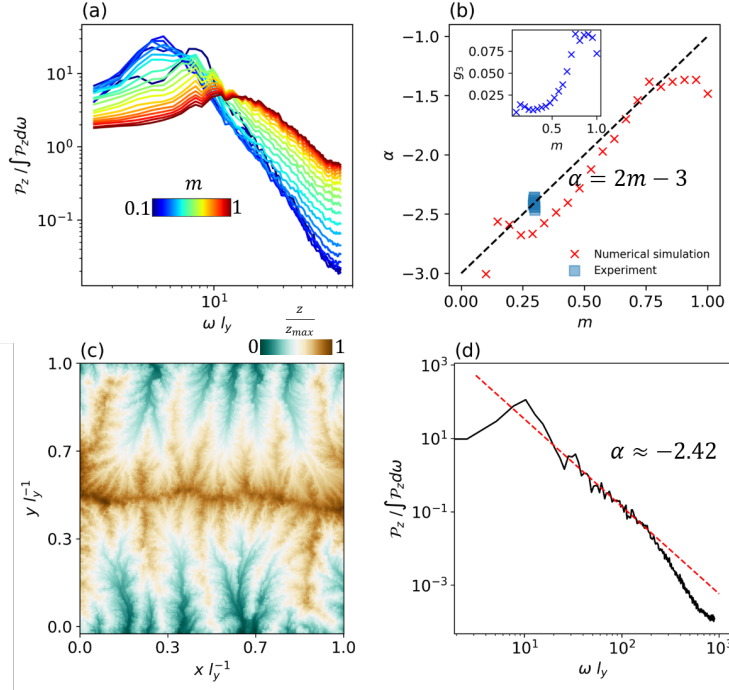


Figure 4. The power spectrum in numerical simulations. (a) shows the PSD of z at the intermediate distance from the boundary ($0.07 \leq y l_y^{-1} \leq 0.27$) for different values of m from numerical simulation. Each line is the average PSD of the signal for $0.07 \leq y l_y^{-1} \leq 0.27$. (b) shows the slope of power fit to the declining part of the PSD from simulations with $\mathcal{C}_T \geq 10^5$, denoted by α as function of the exponent m . The data from the physical experiment are also shown. The black line is the relation $\alpha = 2m - 3$ derived from dimensional and self-similarity arguments in Eq. (8). (c) shows an example of the experimental landscape with $l_y = 500$ mm. (d) shows the PSD computed from the elevation signal at the intermediate distance from the boundary ($0.1 \leq y l_y^{-1} \leq 0.3$). The exponent of power fit is $\alpha = -2.42$ from regression analysis.

5 Power Spectra of Laboratory Experiments

Topographic surfaces from a physical experiment performed at the St. Anthony Falls Laboratory at the University of Minnesota using the eXperimental Landscape Evolution (XLE) facility (Singh et al., 2015; Hooshyar, Singh, et al., 2019) are analyzed. The experiment domain was a 500 mm long 500 mm wide sediment box with a closed-boundary at the sides (vertical boundaries in Fig. 4c) and open-boundary at the top and the bottom (horizontal boundaries in Fig. 4c). Details of the experimental setup can be found elsewhere (Singh et al., 2015). Here, results from ten snapshots of the landscape are shown. These snapshots are taken at 5 minutes intervals at the dynamic steady-state condition

in which the uplift was in balance with total erosion. Fig. 4c shows an example of the normalized elevation field. We used the method proposed by (Perron et al., 2009) to estimate the parameters in Eq. (1). The values of m for the surfaces range from 0.29 to 0.3 (see (Hooshyar, Bonetti, et al., 2019) for details). We computed the exponent of power decay α by regression analysis of the average PSD at the intermediate distance from the boundary ($0.1 \leq y l_y^{-1} \leq 0.3$) as shown in Fig. 4d for the surface in Fig. 4c. The exponent α ranges from -2.49 to -2.39 for the ten surfaces analyzed here. The data points (m, α) are shown in Fig. 4b, which are in agreement with the prediction from the dimensional and self-similarity arguments.

6 Conclusion

Spectral analysis of longitudinal landscape elevation series has been used in a plethora of applications that vary from the theoretical to the operational (Perron, Kirchner, & Dietrich, 2008; Pelletier, 2013). The elevation spectrum contains a peak corresponding to a characteristic length scale beyond which the energy content across wavenumbers drops following a power-law scaling with a characteristic exponent α . The analysis reported here has connected such an exponent α to the basic erosion model parameter m , and in turn, to landscape typology. Specific drainage area exponent m in the erosion term is routinely used to distinguish between the steep landscapes with debris-flow-dominated channels (smaller m) and relatively flat fluvial landscapes (larger m) (Montgomery & Foufoula-Georgiou, 1993; Hooshyar et al., 2017).

Several studies of the elevation spectrum reported exponents near $\alpha = -2$ (Newman & Turcotte, 1990; Huang & Turcotte, 1989; Passalacqua et al., 2006), which corresponds to a fractal dimension $D_m = 1.5$ (Huang & Turcotte, 1989; Voss, 1985) and to fractional Brownian noise. This α value was connected to $m = 0.5$ in the erosion law using self-similarity and dimensional analysis ($\alpha = 2m - 3$). Interestingly, $m = 0.5$ also corresponds to the base case in the Optimal Channel Network theory (Rodríguez-Iturbe & Rinaldo, 2001; Hooshyar et al., 2020), which reproduces several scaling laws of natural basins.

A minimalist model in detachment-limited conditions was employed for the numerical simulations and validation of the results. Besides the dimensions of the main governing variables and parameters, no additional information from the model equation was used in the dimensional analysis; thus, one can expect these results to remain valid for different landscape evolution models (e.g., transport limited or hybrids between transport and detachment limited (Smith & Bretherton, 1972; Willgoose et al., 1991; Davy & Lague, 2009)).

Although the power-scaling in the elevation spectrum persists for a range of channelization index \mathcal{C}_T , the explicit relation between its exponent α and m was achieved in the asymptotic case of very high \mathcal{C}_T . Similarly, scaling laws in other non-equilibrium systems such as fluid turbulence and critical phenomena often arise only asymptotically (Stauffer et al., 1982; Townsend, 1980) (this was humorously labeled 'asymptopia' by R.A. Ferrell (Stauffer et al., 1982)). Thus, on the one hand, finite-size effects, boundary conditions, and other 'impurities' will alter or restrict both the emergence and reliable estimation of power-laws (here α). On the other hand, a known spectral scaling of landscape elevation, especially in its relation to the model parameters, could be profitably utilized in developing efficient numerical simulations of the landscape evolution (Passalacqua et al., 2006). Such numerical schemes would potentially resemble Large-eddy simulation methods used in fluid turbulence (Pope, 2001), where the unsolved dynamics at finer scales are approximated by extrapolating the PSD and can facilitate large-scale simulations of landscape evolution under future scenarios of natural and anthropogenic changes.

Acknowledgments

A.P. acknowledges support from the US National Science Foundation (NSF) grants EAR-1331846 and EAR-1338694, and BP through the Carbon Mitigation Initiative (CMI) at Princeton University. M.H acknowledges support from the Princeton Institute for International and Regional Studies (PIIRS) and the Princeton Environmental Institute (PEI). The physical experiments are originally performed by (Singh et al., 2015) and the data are available through (Hooshyar, Singh, et al., 2019). The link to the simulation code used in this work is provided in (Anand et al., 2019). The numerical simulations in this article were performed on computational resources provided by Princeton Research Computing, a consortium of groups including the Princeton Institute for Computational Science and Engineering (PICSciE) and the Office of Information Technology's High Performance Computing Center and Visualization Laboratory at Princeton University.

7 Appendix I: Locally Isotropic Landscapes

The assumption of local isotropy allowed unifying two length scales L_x and L_y and was essential to deriving Eq. 8. Here, we elaborate on the assumption of the landscape isotropy in relation to the direction of water flow over the surface that is assumed to be in the direction of the surface gradient (i.e., $\frac{\nabla z}{|\nabla z|}$). Fig. 5 shows the distribution of flow direction in small ($a \leq l_y$) and large ($a > l_y$) channels that are subjectively defined for demonstration. In the vicinity of the boundaries (red area in Fig. 5a) the flow directions are aligned towards the boundary both in small and large channels, as shown in the distribution of gradient direction in Fig. 5b. At an intermediate distance from the boundary (the gray area in Fig. 5a) the effect of the boundary partially vanishes at small scales as the flow directions are 'almost' uniformly distributed, although the flow at large scales is strongly aligned towards the boundary Fig. 5c. This observation hints at the validity of the assumption of local isotropy at small scales, which was the basis of the dimensional and self-similarity arguments used to arrive at the relation between α and m .

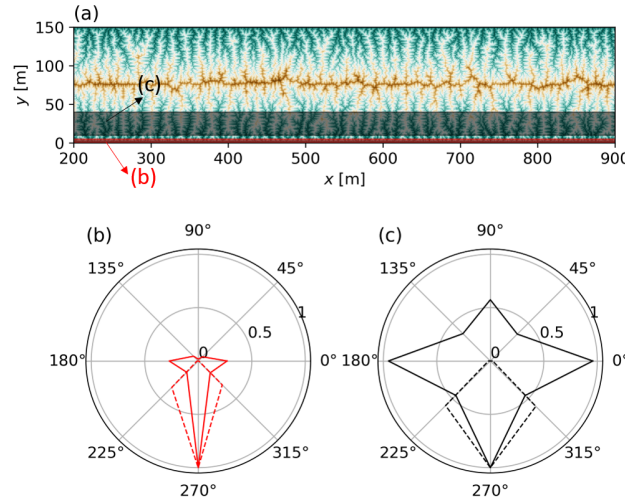


Figure 5. The distribution of flow direction ($\frac{\nabla z}{|\nabla z|}$) in vicinity of the boundary (b) and intermediate distance from the boundary (c). These regions are marked in (a) by red and gray, respectively. The distributions are shown for small ($a \leq l_y$) and large ($a > l_y$) channels.

References

- Anand, S. K., Hooshyar, M., & Porporato, A. (2019). Linear layout of multiple flow-direction networks for landscape-evolution simulations. *arXiv preprint arXiv:1909.03176*.
- Arneodo, A., Argoul, F., Bacry, E., Muzy, J., & Tabard, M. (1992). Golden mean arithmetic in the fractal branching of diffusion-limited aggregates. *Physical review letters*, 68(23), 3456.
- Banavar, J. R., Colaioni, F., Flammini, A., Giacometti, A., Maritan, A., & Rinaldo, A. (1997). Sculpting of a fractal river basin. *Physical review letters*, 78(23), 4522.
- Banavar, J. R., Colaioni, F., Flammini, A., Maritan, A., & Rinaldo, A. (2001). Scaling, optimality, and landscape evolution. *Journal of Statistical Physics*, 104(1-2), 1–48.
- Barenblatt, G., & Goldenfeld, N. (1995). Does fully developed turbulence exist? reynolds number independence versus asymptotic covariance. *Physics of fluids*, 7(12), 3078–3082.
- Barenblatt, G. I. (1996). *Scaling, self-similarity, and intermediate asymptotics: dimensional analysis and intermediate asymptotics* (Vol. 14). Cambridge University Press.
- Bell Jr, T. (1975). Statistical features of sea-floor topography. In *Deep sea research and oceanographic abstracts* (Vol. 22, pp. 883–892).
- Berg-Sørensen, K., & Flyvbjerg, H. (2004). Power spectrum analysis for optical tweezers. *Review of Scientific Instruments*, 75(3), 594–612.
- Bonetti, S., Bragg, A., & Porporato, A. (2018). On the theory of drainage area for regular and non-regular points. *Proceedings of the Royal Society A: Mathematical, Physical and Engineering Sciences*, 474(2211), 20170693.
- Bonetti, S., Hooshyar, M., Camporeale, C., & Porporato, A. (2020). Channelization cascade in landscape evolution. *Proceedings of the National Academy of Sciences*.
- Bonetti, S., Manoli, G., Manes, C., Porporato, A., & Katul, G. G. (2017). Manning’s formula and strickler’s scaling explained by a co-spectral budget model. *Journal of Fluid Mechanics*, 812, 1189–1212.
- Davy, P., & Lague, D. (2009). Fluvial erosion/transport equation of landscape evolution models revisited. *Journal of Geophysical Research: Earth Surface*, 114(F3).
- Goldenfeld, N., & Shih, H.-Y. (2017). Turbulence as a problem in non-equilibrium statistical mechanics. *Journal of Statistical Physics*, 167(3-4), 575–594.
- Hooshyar, M., Anand, S., & Porporato, A. (2020). Variational analysis of landscape elevation and drainage networks. *Proceedings of the Royal Society A*, 476(2239), 20190775.
- Hooshyar, M., Bonetti, S., Singh, A., Foufoula-Georgiou, E., & Porporato, A. (2019). From turbulence to landscapes: Universality of logarithmic mean profiles in bounded complex systems. *arXiv preprint arXiv:1909.13367*.
- Hooshyar, M., Singh, A., & Wang, D. (2017). Hydrologic controls on junction angle of river networks. *Water Resources Research*, 53(5), 4073–4083.
- Hooshyar, M., Singh, A., Wang, D., & Foufoula-Georgiou, E. (2019). Climatic controls on landscape dissection and network structure in the absence of vegetation. *Geophysical Research Letters*, 46(6), 3216–3224.
- Horton, R. E. (1945). Erosional development of streams and their drainage basins; hydrophysical approach to quantitative morphology. *Geological Society of America Bulletin*, 56(3), 275–370.
- Howard, A. D. (1994). A detachment-limited model of drainage basin evolution. *Water resources research*, 30(7), 2261–2285.
- Huang, J., & Turcotte, D. (1989). Fractal mapping of digitized images: application to the topography of arizona and comparisons with synthetic images. *Journal*

- of *Geophysical Research: Solid Earth*, 94(B6), 7491–7495.
- Izumi, N., & Parker, G. (1995). Inception of channelization and drainage basin formation: upstream-driven theory. *Journal of Fluid Mechanics*, 283, 341–363.
- Kramer, S., & Marder, M. (1992). Evolution of river networks. *Physical Review Letters*, 68(2), 205.
- Montgomery, D. R., & Foufoula-Georgiou, E. (1993). Channel network source representation using digital elevation models. *Water Resources Research*, 29(12), 3925–3934.
- Newman, W. I., & Turcotte, D. L. (1990). Cascade model for fluvial geomorphology. *Geophysical Journal International*, 100(3), 433–439.
- Passalacqua, P., Porté-Agel, F., Foufoula-Georgiou, E., & Paola, C. (2006). Application of dynamic subgrid-scale concepts from large-eddy simulation to modeling landscape evolution. *Water Resources Research*, 42(6).
- Pelletier, J. D. (2013). A robust, two-parameter method for the extraction of drainage networks from high-resolution digital elevation models (dems): Evaluation using synthetic and real-world dems. *Water Resources Research*, 49(1), 75–89.
- Perron, J. T., Dietrich, W. E., & Kirchner, J. W. (2008). Controls on the spacing of first-order valleys. *Journal of Geophysical Research: Earth Surface*, 113(F4).
- Perron, J. T., Kirchner, J. W., & Dietrich, W. E. (2008). Spectral signatures of characteristic spatial scales and nonfractal structure in landscapes. *Journal of Geophysical Research: Earth Surface*, 113(F4).
- Perron, J. T., Kirchner, J. W., & Dietrich, W. E. (2009). Formation of evenly spaced ridges and valleys. *Nature*, 460(7254), 502.
- Pope, S. B. (2001). *Turbulent flows*. IOP Publishing.
- Rinaldo, A., Maritan, A., Colaiori, F., Flammini, A., Rigon, R., Rodriguez-Iturbe, I., & Banavar, J. R. (1996). Thermodynamics of fractal networks. *Physical review letters*, 76(18), 3364.
- Rodríguez-Iturbe, I., & Rinaldo, A. (2001). *Fractal river basins: chance and self-organization*. Cambridge University Press.
- Sinclair, K., & Ball, R. C. (1996). Mechanism for global optimization of river networks from local erosion rules. *Physical Review Letters*, 76(18), 3360.
- Singh, A., Reinhardt, L., & Foufoula-Georgiou, E. (2015). Landscape reorganization under changing climatic forcing: Results from an experimental landscape. *Water Resources Research*, 51(6), 4320–4337.
- Smith, T. R., & Bretherton, F. P. (1972). Stability and the conservation of mass in drainage basin evolution. *Water Resources Research*, 8(6), 1506–1529.
- Stauffer, D., Coniglio, A., & Adam, M. (1982). Gelation and critical phenomena. In *Polymer networks* (pp. 103–158). Springer.
- Strahler, A. N. (1952). Hypsometric (area-altitude) analysis of erosional topography. *Geological Society of America Bulletin*, 63(11), 1117–1142.
- Sweeney, K., Roering, J., & Ellis, C. (2015). Experimental evidence for hillslope control of landscape scale. *Science*, 349(6243), 51–53.
- Tennekes, H., Lumley, J. L., Lumley, J., et al. (1972). *A first course in turbulence*. MIT press.
- Townsend, A. (1980). *The structure of turbulent shear flow*. Cambridge university press.
- Turcotte, D. L. (1987). A fractal interpretation of topography and geoid spectra on the earth, moon, venus, and mars. *Journal of Geophysical Research: Solid Earth*, 92(B4), E597–E601.
- Voss, R. F. (1985). Random fractal forgeries. In *Fundamental algorithms for computer graphics* (pp. 805–835). Springer.
- Willgoose, G., Bras, R. L., & Rodriguez-Iturbe, I. (1991). A coupled channel network growth and hillslope evolution model: 1. theory. *Water Resources Research*, 27(7), 1671–1684.

407 Witten, T. A., & Sander, L. M. (1983). Diffusion-limited aggregation. *Physical Re-*
408 *view B*, 27(9), 5686.